Smart Structures and Systems, *Vol. 18, No. 6 (2016) 1217-1231*
DOI: http://dx.doi.org/10.12989/sss.2016.18.6.1217

Battery-free slotted patch antenna sensor for wireless strain and crack monitoring

Xiaohua Yi[1], Chunhee Cho[1], Yang Wang[*1] and Manos M. Tentzeris[2]

[1]*School of Civil and Environmental Engineering, Georgia Institute of Technology, Atlanta, GA 30332, USA*
[2]*School of Electrical and Computer Engineering, Georgia Institute of Technology, Atlanta, GA 30332, USA*

(Received March 14, 2015, Revised September 28, 2016, Accepted October 7, 2016)

Abstract. In this research, a slotted patch antenna sensor is designed for wireless strain and crack sensing. An off-the-shelf RFID (radiofrequency identification) chip is adopted in the antenna sensor design for signal modulation. The operation power of the RFID chip is captured from wireless reader interrogation signal, so the sensor operation is completely battery-free (passive) and wireless. For strain and crack sensing of a structure, the antenna sensor is bonded on the structure surface like a regular strain gage. Since the antenna resonance frequency is directly related with antenna dimension, which deforms when strain occurs on the structural surface, the deformation/strain can be correlated with antenna resonance frequency shift measured by an RFID reader. The slotted patch antenna sensor performance is first evaluated through mechanics-electromagnetics coupled simulation. Extensive experiments are then conducted to validate the antenna sensor performance, including tensile and compressive strain sensing, wireless interrogation range, and fatigue crack sensing.

Keywords: antenna sensor; battery-free; crack sensing; strain sensing; RFID; slotted patch

1. Introduction

Wireless sensing systems have been widely adopted for various applications in today's world (Akyildiz, Su *et al.* 2002). One emerging field of wireless sensing applications is structural health monitoring (Lynch and Loh 2006). To wirelessly measure strain on a structural surface, the typical solution is to connect a regular metal foil strain gage with a wireless sensing device (Kane, Zhu *et al.* 2014). Although the wireless sensing technology reduces system installation time and cost, particularly for large structures like bridges and buildings, they usually require external power supply for operation. This is not convenient for long term monitoring.

Other researchers have recently proposed passive wireless sensors for structural monitoring. In terms of strain sensing, battery-free (passive) strain sensors based on inductive coupling are proposed (Butler, Vigliotti *et al.* 2002, Jia, Sun *et al.* 2006, Loh, Lynch *et al.* 2008). The interrogation distance achieved by inductive coupling is usually limited to several inches, which is inconvenient for practical applications. Similarly, Matsuzaki, Melnykowycz *et al.* (2009) proposed a half wave-length dipole antenna to detect damage in carbon fiber-reinforced polymer (CFRP)

*Corresponding author, Associate Professor, E-mail: yang.wang@ce.gatech.edu

http://www.techno-press.org/?journal=sss&subpage=8 ISSN: 1738-1584 (Print), 1738-1991 (Online)

structures. The damage introduced antenna property changes, including power spectrum and return loss, which are measured and used as the damage indicator. In addition, a circular patch antenna sensor has been proposed for omnidirectional strain sensing by wirelessly measuring scattering parameter (Daliri, Galehdar *et al.* 2012). Another passive strain sensor example is an on-chip RF-MEMS device developed for bio-medical application (Melik, Pergoz *et al.* 2008). Although different types of antennas can be designed, such as dipole antenna(Matsuzaki, Melnykowycz *et al.* 2009), circular patch antenna (Daliri, Galehdar *et al.* 2012), and on-chip antenna (Melik, Pergoz *et al.* 2008), the sensor can only operate in the near field of a reader antenna if no proper signal modulation scheme is adopted. As a result, the wirelessly received sensor signal is mixed with background reflection; only limited interrogation distance is achieved.

In order to increase interrogation distance, electromagnetic backscattering techniques have been exploited for wireless strain sensing. For example, a patch antenna has been designed for wireless strain sensing (Xu and Huang 2012), where a phototransistor is adopted for modulating the RF signal backscattered from the antenna sensor. As a result of the modulation, backscattered sensor signal can be distinguished from environmental reflections. However, besides requiring line of sight, the light-switching mechanism is not practical for outdoor application, where light intensity is usually so strong that the phototransistor can be constantly activated and thus, loses ability of switching. As another example, Thomson, Card *et al*. (2009) developed an RF cavity sensor for wireless strain sensing. An external antenna needs to be connected with the cavity sensor for interrogation. Due to the cavity configuration, the sensor is more suitable for embedment inside concrete, instead of installation on a metallic surface. To distinguish sensor signal from environmental noise, signal modulation mechanism is important to ensure a reliable signal-to-noise ratio. Occhiuzzi, Paggi *et al*. (2011) proposed a meander-line RFID (radiofrequency identification) antenna sensor for wireless strain sensing. The shift in the power level is correlated with applied strain to determine structural deformation. Since the power level is susceptible to environmental noise, the measurement accuracy is limited.

Recently, an RFID based folded patch antenna sensor is proposed for wireless strain sensing (Yi, Cho *et al.* 2013b). The proposed folded patch antenna is capable to sense small tensile strains at around 20με, and large strains up to 10,000 με (Yi, Wu *et al.* 2011). The sensor is also capable of capturing fatigue crack propagation (Yi, Cooper *et al.* 2012). The plane dimension of the sensor is 61mm × 69mm, which is still relatively too large to monitor strain/stress concentration in a small hot spot area. In order to further reduce the sensor footprint, a slotted patch antenna sensor is proposed (Yi, Wang *et al.* 2013c, Cho, Yi *et al.* 2014). To thoroughly evaluate the prototype antenna sensor, mechanics-electromagnetics coupled simulation is performed to study the correlation between strain distribution and surface current density distribution. The strain sensing tests are conducted both in tension and compression. The interrogation distance is also evaluated. Finally, besides the strain sensing capability, a special double-crack fatigue test with two simultaneously operating antenna sensors is also conducted.

The rest of this paper is organized as follows. Section II introduces the slotted patch antenna sensor and related sensing mechanism. Section III presents the mechanics-electromagnetics coupled simulation for strain sensing. Section IV describes the experiments conducted to validate the sensor performance, including tension/compressive strain sensing performance, interrogation range, and fatigue crack sensing. Section V provides a summary and discussion of this work.

2. Slotted patch antenna sensor design and strain sensing mechanism

This section describes slotted patch antenna sensor design, followed by strain sensing mechanism of the antenna sensor. Although the folded patch antenna sensor presented in (Yi, Cho *et al.* 2013b) shows good performance for wireless strain sensing, the sensor size is still relatively large (61 mm × 69 mm), especially for strain/stress concentration monitoring in a small hot-spot area. For further size reduction, a slotted patch configuration is proposed. The slotted patch antenna sensor is designed to reduce the sensor footprint by detouring the surface current path (Yi, Cho *et al.* 2013a). Fig. 1 shows a perspective view of the sensor, and the intended surface current paths on the sensor. The surface current is detoured along the slots and vias between top and bottom copper claddings. In other words, the slots in the copper cladding help generate a longer and detoured surface current path, so that the antenna resonance frequency can remain in 900 MHz RFID band, while the plane dimension of the antenna sensor can be reduced to 44 mm × 48 mm. An RFID chip from NXP Semiconductors (Model #: SL3ICS1002) is located at the top center of the sensor for RFID signal modulation. For this slotted patch antenna sensor design, the initial resonance frequency can be estimated as

$$f_{R0} \approx \frac{c}{8(L+L')\sqrt{\beta_{r0}}} \tag{1}$$

where c is the speed of light, L is the length of top copper cladding (L=40 mm in the slotted patch antenna sensor design), L' is the additional sensor length due to fringing effect. The substrate adopted in this research is RT/duroid® 5880 from Rogers Corporation and β_{r0} is the dielectric constant of the substrate, which is 2.2. The thickness of the substrate is 0.79 mm. When the antenna sensor is bonded to a structural surface, the dimension of the sensor deforms together with the monitored structural surface under strain. Assuming the applied strain in the longitudinal direction is ε, the shifted resonance frequency under strain can be estimated as

$$f = \frac{c}{8(1+\varepsilon)(L+L')\sqrt{\beta_{r0}}} = \frac{f_{R0}}{1+\varepsilon} \approx f_{R0}(1-\varepsilon) \tag{2}$$

When the applied strain is small, the resonance frequency change has an approximately linear relationship with applied strain according to Taylor expansion.

Due to the fabrication and installation errors, the initial resonance frequencies of the sensors may be different. In order to accommodate the tolerance, the normalized strain sensitivity can be defined according to the following equation

$$\Delta f_N = \frac{f_R - f_{R0}}{f_{R0}} \approx -\varepsilon \tag{3}$$

where Δf_N represents normalized frequency change, and f_R is the resonance frequency when antenna is under strain ε. Although Eq. (3) shows magnitude of Δf_N approximately equals magnitude of strain ε, in practice, Δf_N usually has a smaller magnitude. The primary reason is that only a percentage of the strain on structural surface is transferred through antenna substrate to the top copper layer of the sensor. This strain transfer effect reduces the achieved strain sensitivity, as described by following equation

$$\Delta f_N = -S_N \tag{4}$$

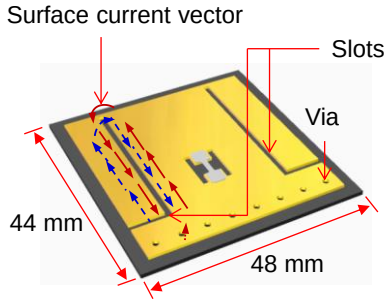

Fig. 1 Illustration of the surface current flows on the slotted patch antenna (blue dashed lines represent current on the bottom surface)

Here S_N is the normalized strain sensitivity with a value close to and less than 1 ppm/με (ppm - parts per million).

3. Multi-physics coupled simulation

After the antenna sensor design, the sensor performance can be validated by mechanics-electromagnetics coupled simulation. Fig. 2 shows the COMSOL simulation model of the passive slotted patch antenna sensor. The sensor is bonded at the center of an aluminum plate. The RFID chip is simulated as a lumped port with the same electrical impedance ($Zc = 13.3 - j$ 122 Ω) as provided by the chip manufacture. The bonding between the bottom copper cladding of the antenna sensor and the aluminum plate is assumed to be ideal, i.e., no relative displacement occurs at the interface. Similarly, bonding between the top/bottom copper cladding and the substrate material is assumed to be ideal. The antenna sensor and the aluminum plate are placed at the center of an air sphere. At the outer surface of the air sphere, boundary condition is set as a perfectly matched layer (PML). The PML boundary condition allows electromagnetic wave emitted by the antenna sensor to pass through with minimal reflections, which mimics the dissipation of electromagnetic wave into infinite free space. The two copper cladding layers, i.e. top and bottom, are meshed using shell elements with a thickness of 0.017 mm. Key mechanical and electromagnetic properties of the materials are summarized in Table 1. Copper and aluminum materials are modelled as perfect electric conductor (PEC) in the electromagnetic simulation.

In the mechanical strain simulation, tetrahedral and prism elements are adopted to model solid structures such as the aluminum specimen and substrate, and to efficiently resolve boundary layers. For modeling shell structures, such as top and bottom copper cladding, triangular elements are used to reduce discretization error and quadrilateral elements are adopted to achieve better numerical accuracy. In the electromagnetic simulation, the air sphere and the PML layer are similarly modelled as tetrahedral and prism elements. Table 2 lists the number of each type of element, and the number of DOFs in COMSOL model. Prescribed displacements are applied at two ends of the aluminum plate, so that five different strain levels (from 0 to 2,000 με at an increment step of 500 με) are generated in the aluminum plate. The simulated frequency range is 909~915 MHz with a frequency step of 0.1 MHz. The resonance frequency is finally determined

by picking the lowest peak of the S11 plot. Table 2 lists the number of each element type, and the number of DOFs in COMSOL model. The average computation time for one frequency point is about 8 minutes and 18 seconds. The total computation time is also related with total number of frequency points and strain steps. For 5 strain steps and 61 frequency points, the total time is 42 hours and 12 minutes. The required memory for the computation in the electromagnetic frequency domain solver is around 2.5 GB, which is reasonable.

Fig. 3(a) presents simulated strain distribution in the longitudinal (y-direction) direction on the aluminum plate and the antenna sensor, when the applied strain in the plate is 2,000 με. Approximately uniform strain distribution is achieved around the center of the aluminum plate. On the other hand, the strain distribution on top copper cladding has large variations that are highly dependent on the slotted pattern. Fig. 3(b) shows the surface current density distribution in y-direction on the top copper cladding. The corresponding mechanical strain for Fig. 3(b) is 2,000 με and the related resonance frequency is 910.8 MHz. The figure clearly shows the surface current density detouring along the slots and the vias, which as intended enables sensor size reduction.

Fig. 4(a) shows simulated S11 plots at different strain levels. As expected, the resonance frequency of the antenna sensor reduces as the strain increases. The normalized resonance frequency is plotted against strain in Fig. 4(b). The normalized strain sensitivity is –0.784 ppm/με, which means 1 με generated on the aluminum specimen causes the resonance frequency to decrease by 0.784 ppm. The coefficient of determination (R^2) is 0.9999, which indicates an excellent linearity.

Table 1 Key properties of the materials used in COMSOL simulation model

	Substrate	**Copper cladding**	**Aluminum**
Material type	Glass microfiber reinforced PTFE	Copper	6061 Aluminum alloy
Relative permittivity (β_{r0})	2.2	1	1
Conductivity (S/m)	0.5×10^{-9}	PEC	PEC
Poisson's ratio	0.4	0.35	0.33
Young's modulus (GPa)	1.07	110	69

Table 2 Number of elements and degrees of freedom in the slotted patch antenna sensor model

Number of Elements		**Number of DOFs**	
Tetrahedron	39,665	Mechanics	53,124
Prism	3,220		
Triangle	5,768	Electromagnetics	477,429

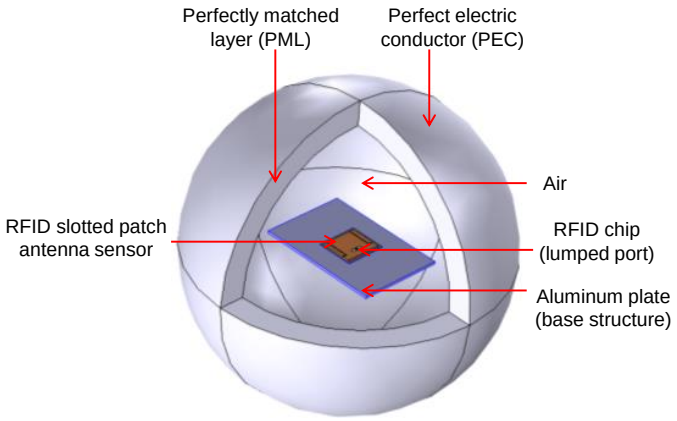

Fig. 2 Multi-physics simulation model of slotted patch antenna sensor using COMSOL

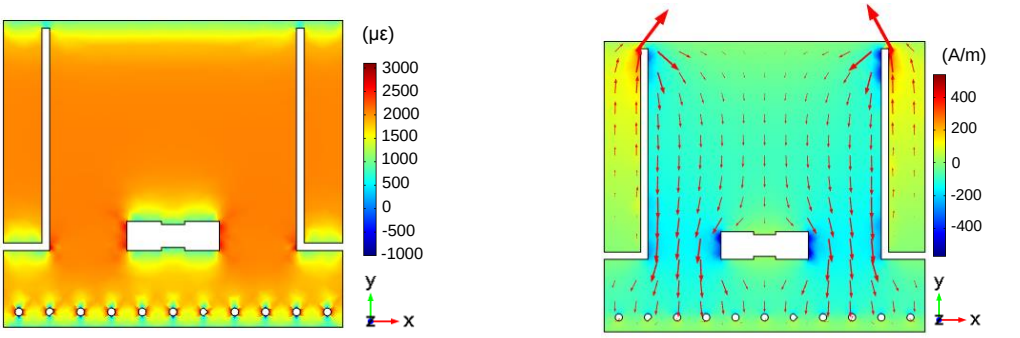

(a) Strain distribution in y-direction (b) Surface current density in y-direction

Fig. 3 Field distributions from mechanics-electromagnetics coupled simulation

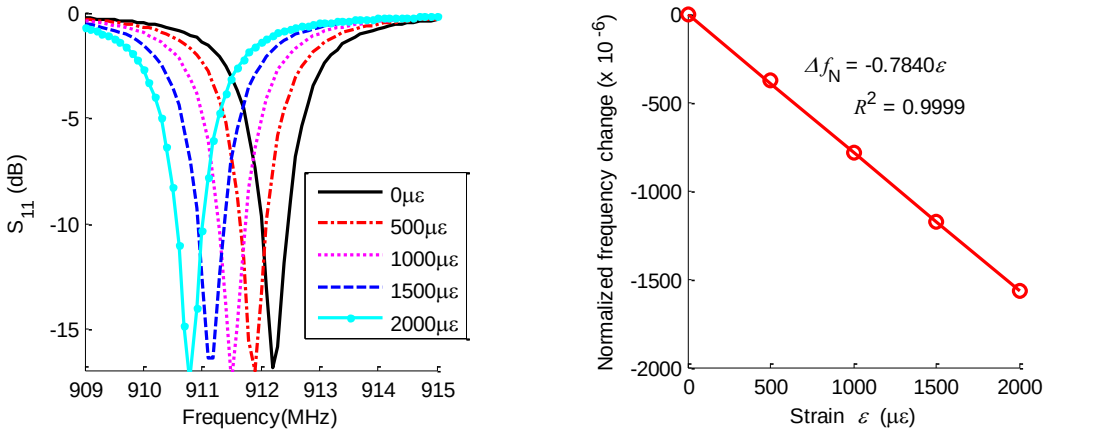

(a) S_{11} parameter (b) Normalized resonance frequency change Δf_N versus strain ε (f_{R0} = 912.2 MHz)

Fig. 4 Strain simulation results of the passive slotted antenna sensor from COMSOL

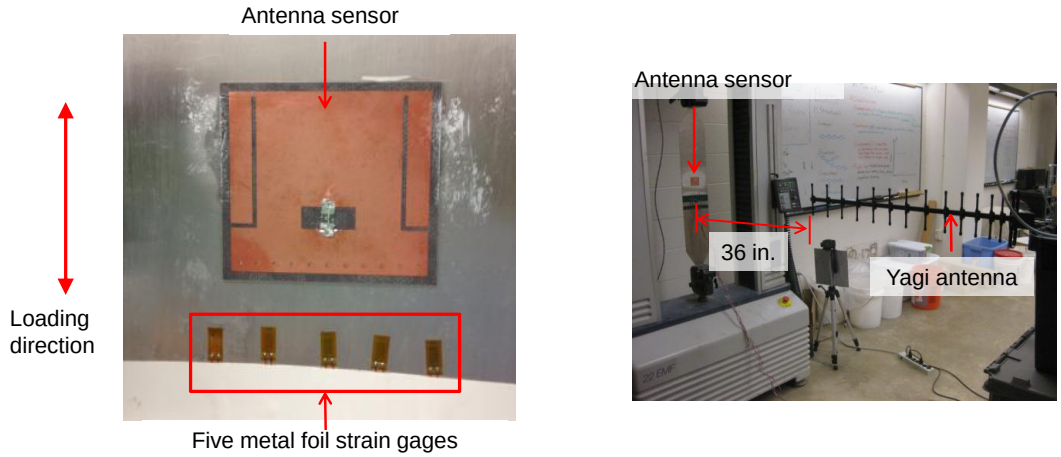

(a) Sensor instrumentation on an aluminum specimen (b) Wireless strain sensing experiment

Fig. 5 Experimental setup for a tensile test with 36 in. interrogation distance

4. Wireless strain sensing results

To evaluate sensor performance, extensive experiments are conducted to evaluate sensor performance. Section 4.1 presents test results of strain sensing under tension, followed by results under compression in Section 4.2. Section 4.3 presents wireless interrogation range. Section 4.4 shows fatigue crack sensing results.

4.1 Strain sensing performance under tension

This section describes the tensile strain sensing performance of the passive slotted patch antenna sensor. The experimental setup is shown in Fig. 5. During this experiment, a Tagformance reader from Voyanic Ltd. is adopted as the wireless interrogation reader. The interrogation power from the reader is varied in order to determine minimum power required to activate the RFID chip. This minimum interrogation power is also named as interrogation power threshold. The interrogation power and frequency resolutions in the experiments are 0.1 dBm and 0.1 MHz, respectively. The reader antenna is an 18 dBi high-gain Yagi antenna and the interrogation distance is 36 in. The tensile load is configured so that approximately 20 με increment is achieved at each loading step.

The interrogation power threshold plot is shown in Fig. 6(a). Eleven strain levels are tested. For clarity, interrogation power threshold plots for only four strain levels are illustrated in Fig. 6(a). The figure clearly demonstrates that as strain level increases, the S11 curve shifts towards left, indicating a reducing resonance frequency. Fig. 6(b) shows the normalized strain sensitivity is –0.6811 ppm/με when the interrogation distance is 36 in. The measured strain sensitivity is smaller than the simulated sensitivity as presented in Fig. 4(b). This is probably due to the strain transfer effect between aluminum and top copper cladding of the sensor. In the

mechanics-electromagnetics coupled simulation, bonding between copper cladding and aluminum plate is assumed to be ideal. This is not the case in the experiment installation, due to imperfect bonding of super glue. The corresponding coefficient of determination is 0.9857, which still indicates acceptable linearity.

4.2 Strain sensing performance under compression

This section describes the compression strain sensing test of the passive slotted patch antenna sensor. A judiciously devised compression setup is shown in Fig. 7(a), with a tapered aluminum specimen designed to generate constant compressive strain on the surface. The compression setup includes one strong base plate with a pair of bearings in the middle of the front side. The specimen fits between the base plate and the bearings. To generate compression strain on the specimen, two bolts through the upper and lower ends of the base plate are screwed towards the specimen that is constrained by bearings in the middle. The passive slotted patch antenna sensor is installed in the middle of the specimen, together with five metal foil strain gages for comparison. The reader antenna is an 18 dBi high-gain Yagi antenna as shown in Fig. 7(b). The interrogation distance is 36 in. The two blots are turned so that approximately 50 με more compression is achieved at each loading step. All other experimental setups and data analysis remain the same as before.

Seven strain levels are tested. For clarity, interrogation power threshold plots of only four strain levels are illustrated in Fig. 8(a). Fig. 8(b) shows the normalized strain sensitivity is –0.8706 ppm/με when the interrogation distance is 36 in.

The larger compression sensitivity compared with the tensile sensitivity in Fig. 4(b) can be explained by the three-point compression setup. When the antenna sensor is bent with the aluminum specimen, the distance from neutral axis to antenna top surface is longer than that to the aluminum specimen surface, which implies that strain on the antenna sensor surface is higher than that on the aluminum specimen. The larger experienced strain on the top layer of the antenna sensor introduces larger resonance frequency shift and thus larger compression strain sensitivity. The corresponding coefficient of determination is 0.9967, which indicates acceptable linearity.

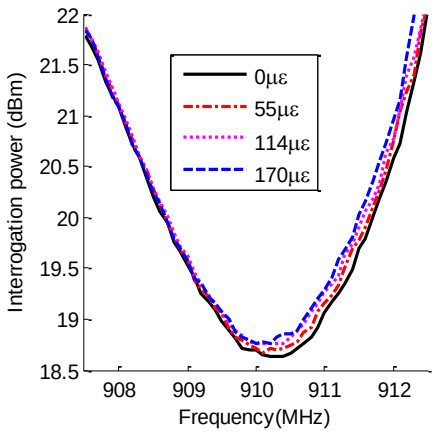

(a) Average interrogation power threshold

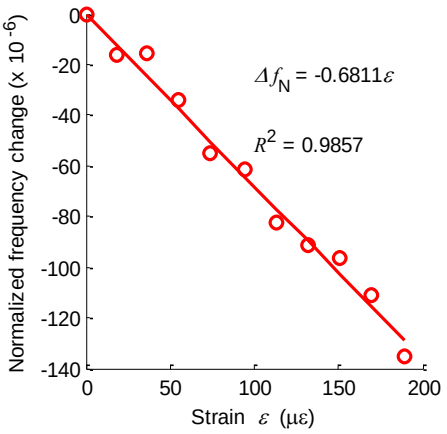

(b) Normalized resonance frequency change Δf_N versus strain ε (f_{R0} = 910.239 MHz)

Fig. 6 Tensile testing results at 36 in. interrogation distance

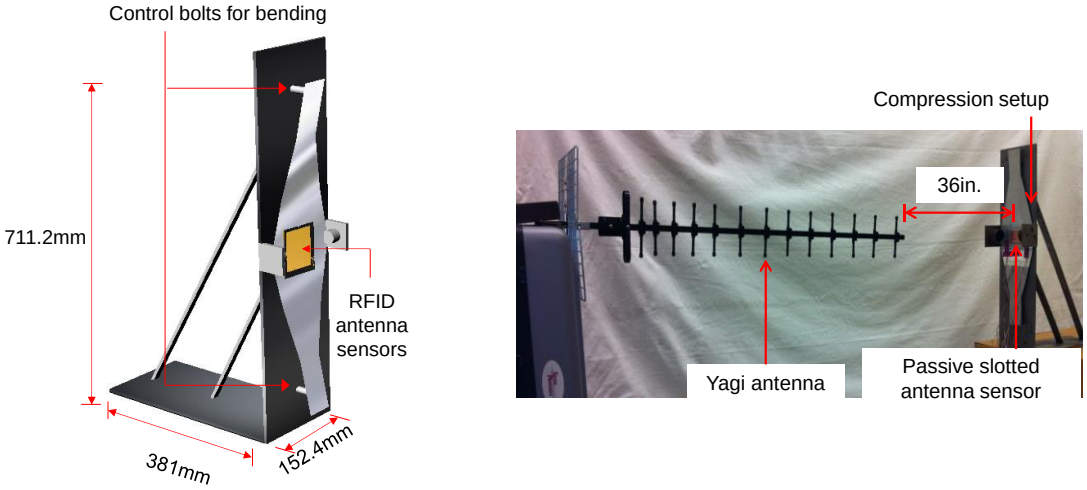

(a) Setup drawing (b) Experimental setup

Fig. 7 Compression testing at 36 in. interrogation distance

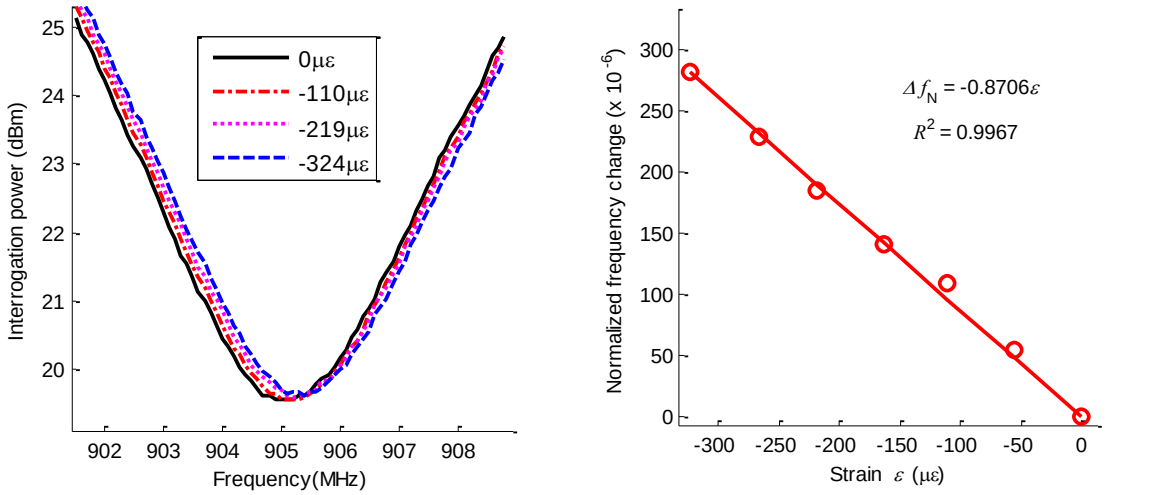

(a) Average interrogation power threshold

(b) Normalized resonance frequency change Δf_N versus strain ε

Fig. 8 Compressive testing results at 36 in. interrogation distance

4.3 Wireless interrogation range

This section describes wireless interrogation range test. The reader antenna used in the testing is an 18 dBi high-gain Yagi antenna. Fig. 9 shows the experimental setup for the interrogation range test. The Yagi reader antenna faces the wireless strain sensor, and the distance between the

sensor and the reader antenna is gradually increased from 12 in. up to 90 in. The reader antenna is connected with Tagformance reader. The interrogation power threshold is recorded by the reader at different interrogation distances.

The interrogation power from the Tagformance reader at different interrogation distances are plotted in Fig. 10. When the interrogation distance is 12 in., the interrogation power threshold around the resonance frequency is less than 12 dBm, meaning a low interrogation power is needed to activate the passive sensor. When the interrogation distance is increased up to 90 in., the reader is still capable of measuring 3dB bandwidth (needed for reliably extracting resonance frequency) of the interrogation power curve. The power level around the resonance frequency increases to about 23 dBm, i.e., larger interrogation power is needed at a longer distance.

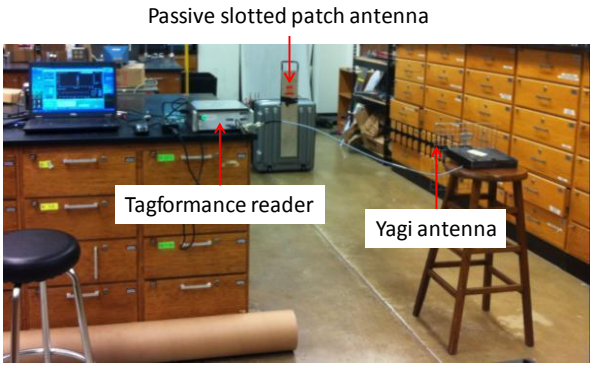

Fig. 9 Experimental setup for the interrogation distance test

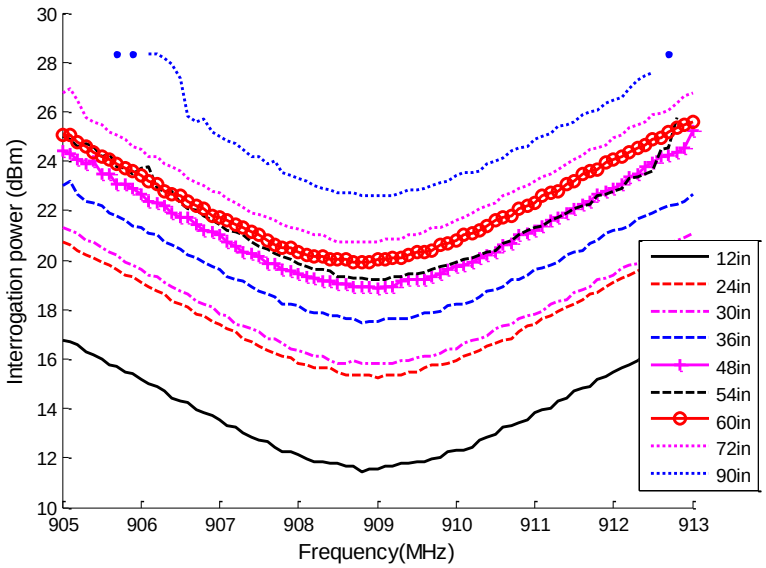

Fig. 10 Interrogation power at different interrogation distances

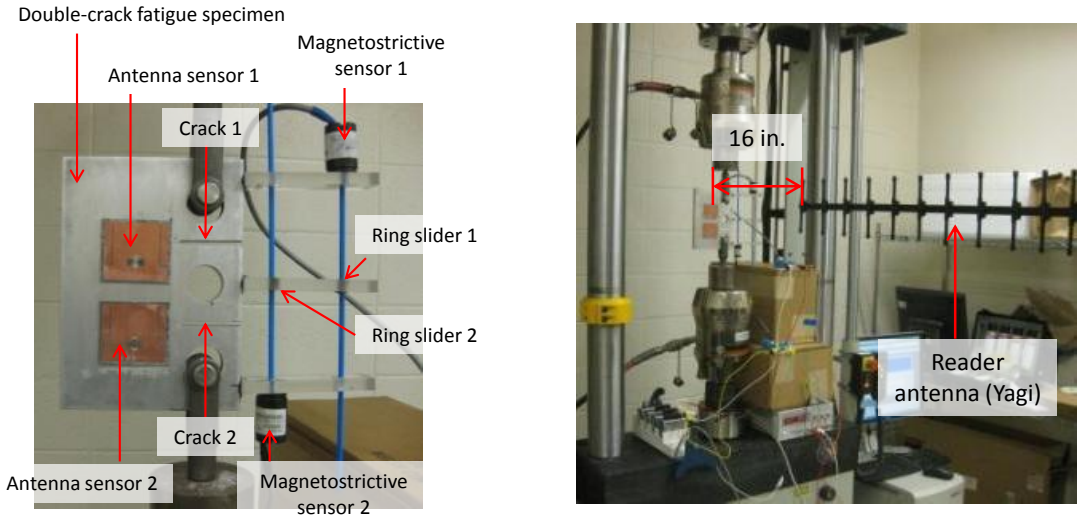

(a) Fatigue specimen (b) Experimental setup

Fig. 11 Experimental setup for the fatigue test of passive slotted-patch antenna sensor

4.4 Fatigue crack sensing

Fatigue crack test with a double-crack aluminum specimen has been conducted to investigate crack monitoring performance of the slotted patch antenna sensor. Fig. 11 shows the specimen configuration and experimental setup for fatigue crack test. Antenna sensors #1 and #2 are installed along the crack propagation paths of upper and lower notches, respectively. To measure crack opening of the specimen during cyclic loading, one magnetostrictive position sensor from MTS Sensors (CS-194-AV) is installed across each notch. The sensor provides the position of a magnetic ring slider along a 19.4 cm stroke.

Magnetostrictive sensor #1 measures upper crack opening, and magnetostrictive sensor #2 measures lower crack opening. The applied cyclic loading is 5 Hz sinusoidal wave. The loading range is 1.5~4.5 kips. The specimen is first loaded to generate an initial crack during the pre-crack stage. After pre-crack, the double crack openings of the specimen are measured after every 10,000 loading cycles. During the measurement, the holding load is kept at 3 kips. The reader antenna adopted in this experiment is a 900MHz Yagi antenna, which is placed 16 in. away from the center of the double-crack specimen, as shown in Fig. 11(b).

The fatigue test continues until the specimen broke through crack #1 and antenna sensor #1 debonds from the specimen, which occurs after loading stage #10. Fig. 12 shows representative photos of the specimen at three loading stages. The top left photo shows the back view of the specimen after pre-crack loading stage. The two initial cracks are 0.08 in. and 0.11 in. at the upper and lower notches, respectively. The top right photo shows the back view of the specimen after 80,000 loading cycles. The crack lengths are increased to 1.027 in. and 0.787 in. respectively. After this stage, the antenna sensor #1 is debonded from the specimen as shown in the bottom photo and the experiment is ended.

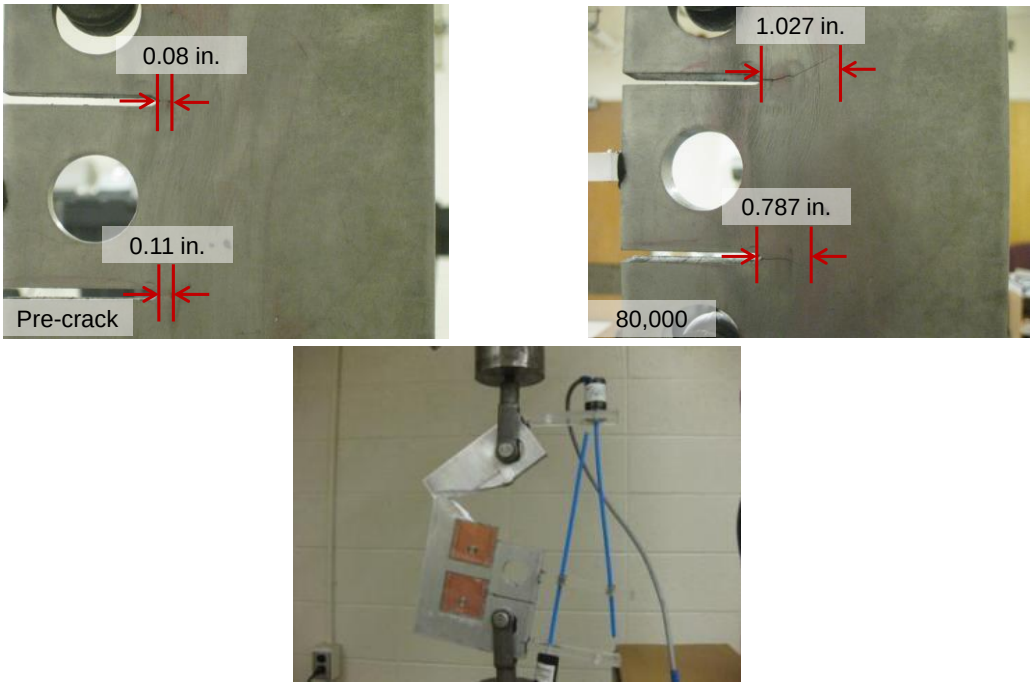

Fig. 12 Photos of double-crack specimen at different crack lengths

Figs. 13(a) and 13(b) plot the average interrogation power thresholds at different crack lengths of two antenna sensors. The resonance frequencies at all crack lengths and widths are extracted, and plotted in Figs. 13(c) and 13(d). Overall, about 1.5 MHz resonance frequency decrease is observed from the antenna sensor #1, when the upper crack length increases to 1.027 in. Such large frequency decrease is relatively easy to measure in practice. However, much smaller resonance frequency is observed at antenna sensor #2, mainly due to the relatively smaller growth of the lower crack. The curves in Figs. 13(c) and 13(d) also show resonance frequency increments when the crack length/width are small. The results indicate that at the beginning of the test, the antenna sensors experience mainly compression rather than tension. This could be explained by initial in-plane bending of the specimen when the testing machine is paused with a static load at 3 kips for taking wireless measurements. Nevertheless, after cracks grow near the antenna sensors, the sensors start experiencing more tension.

5. Conclusions

The passive slotted patch antenna sensor is designed to reduce sensor footprint, while maintaining the sensor operating frequency around 900 MHz RFID band. The size reduction is achieved by introducing slots on the top copper cladding to detour the surface current, the sensor size is reduced to 44 mm × 48 mm, which is only half of the previously proposed folded patch antenna sensor. Mechanics-electromagnetics coupled simulation is first conducted to evaluate the strain sensing sensitivity. Extensive experiments are further performed to verify the sensor

performance. The test results show that the passive slotted patch antenna sensor is capable of sensing small strain levels. The sensor can monitor not only tensile strain, but also compressive strain with the same sensing mechanism. The interrogation range test shows that the sensor can be recognized when the reader is as far as 90 in. away from the sensor. Besides strain sensing, the proposed sensor is also capable of fatigue crack sensing. The crack propagation/stress concentration can be easily tracked by the antenna sensor array.

Although the sensor can be interrogated at a distance of 90 in., it is still relatively limited for field testing in an outdoor application. To further improve the interrogation distance, in future studies, an active slotted patch antenna sensor can be designed by integrating an active RFID chip.

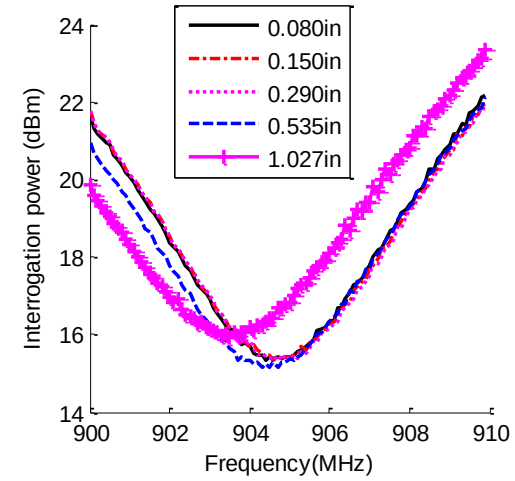

(a) Average interrogation power from antenna sensor #1

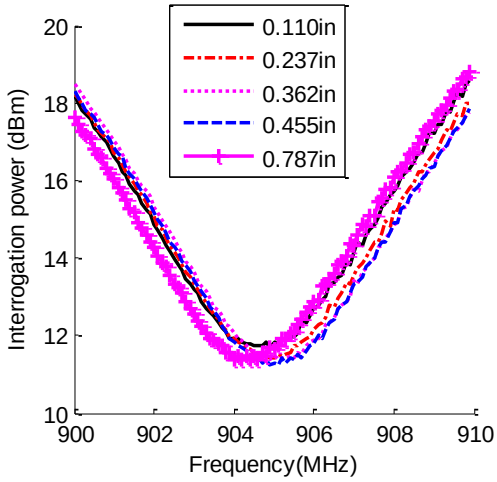

(b) Average interrogation power from antenna sensor #2

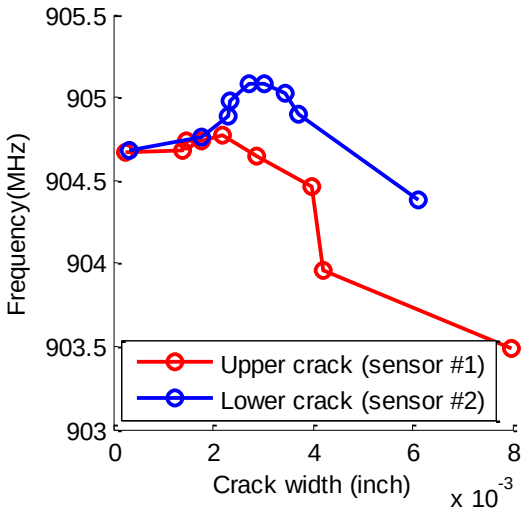

(c) Resonance frequency versus crack width

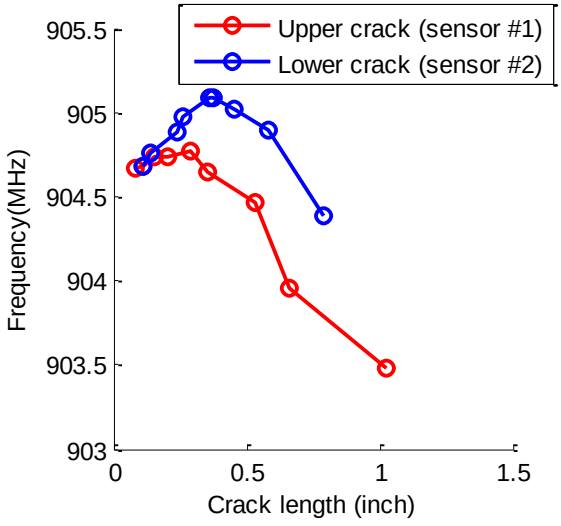

(d) Resonance frequency versus crack length

Fig. 13 Fatigue test results of the passive slotted-patch antenna sensors

Acknowledgments

This material is based upon work supported by the Air Force Office of Scientific Research and Federal Highway Administration. Any opinions, findings, and conclusions or recommendations expressed in this publication are those of the authors and do not necessarily reflect the view of the sponsors.

References

Akyildiz, I.F., Su, W., Sankarasubramaniam, Y. and Cayirci, E. (2002), "Wireless sensor networks: a survey", *Comput. Netw.*, **38**, 393-422.

Butler, J.C., Vigliotti, A.J., Verdi, F.W. and Walsh, S.M. (2002), "Wireless, passive, resonant-circuit, inductively coupled, inductive strain sensor", *Sensor. Actuat. A: Phys.*, **102** (1-2), 61-66

Cho, C., Yi, X., Wang, Y., Tentzeris, M.M. and Leon, R.T. (2014), "Compressive strain sensing measurement using RFID patch antenna sensors", *Proceedings of SPIE, Sensors and Smart Structures Technologies for Civil, Mechanical, and Aerospace System*, San Diego, CA, USA, March 10-14, 2014.

Daliri, A., Galehdar, A., John, S., Wang, C.H., Towe, W.S.T. and Ghorbani, K. (2012), "Wireless strain measurement using circular microstrip patch antennas", *Sensors Actuat. A: Phys.*, **184**, 86-92.

Jia, Y., Sun, K., Agosto, F.J. and Quinones, M.T. (2006), "Design and characterization of a passive wireless strain sensor", *Meas. Sci. Technol.*, **17**(11), 2869-2876.

Kane, M., Zhu, D., Hirose, M., Dong, X., WInter, B., Hackell, M., Lynch, J.P., Wang, Y. and Swartz, A. (2014), "Development of a extensible dual-core wireless sensing node for cyber-physical systems", *Proceedings of SPIE, Sensors and Smart Structures Technologies for Civil, Mechanical, and Aerospace System*, San Diego, CA, USA.

Loh, K.J., Lynch, J.P. and Kotov, N.A. (2008), "Inductively coupled nanocomposite wireless strain and pH sensors", *Smart Struct. Syst.*, **4**(5), 531-548.

Lynch, J.P. and Loh, K.J. (2006), "A summary review of wireless sensors and sensor networks for structural health monitoring", *Shock Vib. Digest*, **38**(2), 91-128.

Matsuzaki, R., Melnykowycz, M. and Todoroki, A. (2009), "Antenna/sensor multifunctional composites for the wireless detection of damage", *Compos. Sci. Technol.*, **69**, 2507-2513.

Melik, R., Pergoz, N.K., Unal, E., Puttlitz, C. and Demir, H.V. (2008), "Bio implantable passive on-chip RF-MEMS strain sensing resonators for orthopedic application", *J. Micromech. Microeng.*, **18**, 115017.

Occhiuzzi, C., Paggi, C. and Marrocco, G. (2011), "Passive RFID strain-sensor based on meander-line antennas", *IEEE T. Antenn. Propag.*, **59** (12), 4836-4840.

Thomson, D.J., Card, D. and Bridges, G.E. (2009), "RF cavity passive wireless sensors with time-domain gating-based interrgoation for SHM of civil structures", *IEEE Sensors J.*, **9**(11), 1430-1438.

Xu, X. and Huang, H. (2012), "Battery-less wireless interrogation of microstrip patch antenna for strain sensing", *Smart Mater. Struct.*, **21**, 125007.

Yi, X., Cho, C., Cook, B., Wang, Y., Tentzeris, M.M. and Leon, R.T. (2013a), "Design and simulation of a slotted patch antenna sensor for wireless strain sensing", *Proceedings of SPIE, Nondestructive Characterization for Composite Materials, Aerospace Engineering, Civil Infrastructure, and Homeland Security*, San Diego, California, USA.

Yi, X., Cho, C., Cooper, J., Wang, Y., Tentzeris, M.M. and Leon, R.T. (2013b), "Passive wireless antenna sensor for strain and crack sensing-electromagnetic modeling, simulation, and testing", *Smart Mater. Struct.*, **22**, 085009.

Yi, X., Cooper, J., Wang, Y., Tentzeris, M.M. and Leon, R.T. (2012), "Wilress crack sensing using an RFID-based folded patch antenna", *Proceeding of the 6th International Conference on Bridge Maintenance, Safety and Management*, Lake Como, Italy.

Yi, X., Wang, Y., Tentzeris, M. M. and Leon, R.T. (2013c), "Multi-physics modeling and simulation of a

slotted patch antenna for wireless strain sensing", *Proceedings of 9th International Workshop on Structural Health Monitoring* Standford, CA, USA.

Yi, X., Wu, T., Lantz, G., Cooper, J., Cho, C., Wang, Y., Tentzeris, M.M. and Leon, R.T. (2011), "Sensing resolution and measurement range of a passive wireless strain sensor", *Proceedings of the 8th International Workshop on Structural Health Monitoring*, Stanford, CA, USA.

CY